Electronic Supplementary Material (ESI) for Chemical Communications.

Supporting Information

Methane dehydroaromatization catalyzed by Mo/ZSM-5: location-steered activity and mechanism

Guanna Li[a,b*]

[a]Biobased Chemistry and Technology, Wageningen University, Bornse Weilanden 9, 6708 WG Wageningen, The Netherlands

[b]Inorganic Systems Engineering, Department of Chemical Engineering, Delft University of Technology, Van der Maasweg 9, 2629 HZ Delft, The Netherlands

Email: guanna.li@wur.nl

Computational details

All spin polarized DFT calculations were performed by using the Vienna Ab initio Simulation Package (VASP, version 5.3.5).[1, 2] The PBE functional based on the generalized gradient approximation was chosen to account for the exchange–correlation energy.[3] A plane-wave basis set in combination with the projected augmented wave (PAW) method was used to describe the valence electrons and the valence-core interactions, respectively.[4] The kinetic energy cut-off of the plane wave basis set was set to 500 eV. Gaussian smearing of the population of partial occupancies with a width of 0.05 eV was used during iterative diagonalization of the Kohn-Sham Hamiltonian. The threshold for energy convergence for each iteration was set to 10^{-5} eV. Geometries were assumed to be converged when forces on each atom were less than 0.05 eV/Å. Considering the large unit cell, Brillouin zone-sampling was restricted to the gamma point. The Van der Waals (vdW) interactions were included by using Grimme's DFT-D3(BJ) method as implemented in VASP.[5]

The nudged-elastic band method with the improved tangent estimate (CI-NEB)[6] was used to determine the minimum energy path and to locate the transition state structure for each elementary reaction step. The maximum energy geometry along the reaction path generated by the CI-NEB method was further optimized using a quasi-Newton algorithm. In this procedure, only the extra-framework atoms were relaxed. Vibrational frequencies were calculated by determining the second derivatives of the Hessian matrix using the density functional perturbation theory as implemented in VASP 5.3.5. The transition state was confirmed by showing a single imaginary frequency corresponding to each reaction coordinate.

The orthogonal MFI unit cell with lattice parameters of a = 20.241 Å, b = 20.015 Å and c = 13.439 Å as optimized by DFT with an all-silica MFI periodic model was used for all calculations. The optimized unit cell parameters agree well with experimental data for calcined ZSM-5.[7] To compensate for the positive charge of the extra-framework cationic molybdenum complexes, two framework Si^{4+} ions at a specific location (α-, β-, γ-, or δ- sites) in the MFI unit cell were substituted by two Al^{3+}. The resulting ZSM-5 model had a Si/Al ratio of 47.

Mean-field microkinetic modeling (MKM) was performed based on the DFT results of all elementary reaction steps to obtain the apparent activation barrier, degree of rate control, and rate-determining steps.[8] All MKM runs were simulated by our home-made script.

The rate constant of each elementary reaction step was calculated by:

$$k = \frac{k_b T}{h} e^{-E_a / RT}$$

The set of ordinary differential equations (ODEs) for the coverage of species i was obtained by:

$$\frac{\partial \theta_i}{\partial_t} = \sum_{\pm j} c_{i,\pm j} r_{\pm j}$$

In which $c_{i,\pm j}$ is the concentration of the species i in the elementary reaction. The +j represents the forward reaction and −j the backward reaction. The $r_{\pm j}$ refers to the rate of the corresponding elementary reaction. The ODEs were solved at the steady state, in which $\partial\theta_i/\partial_t$=0, by using the stiff solver built in Python.

Degree of rate control (DRC) introduced by Campbell[9] indicates the significance of a specific transition state for the overall reaction rate. By changing the energy of the particular transition state of step i while keeping the energy of all other reaction intermediates and transition state constant, the DRC for step i is equal to:

$$X_{RC,i} = \frac{\vec{k}_i}{r}\left(\frac{\partial r}{\partial \vec{k}_i}\right)\Bigg|_{K_{i,ep}, k_{j \neq i}}$$

The magnitude of $X_{RC,i}$ determines how the transition state of step i influencing the overall reaction rate. A negative value indicates that increasing the transition state energy of step i decreases the overall rate, while a positive value indicates that decreasing the transition state energy of step i leads to increase the overall rate.

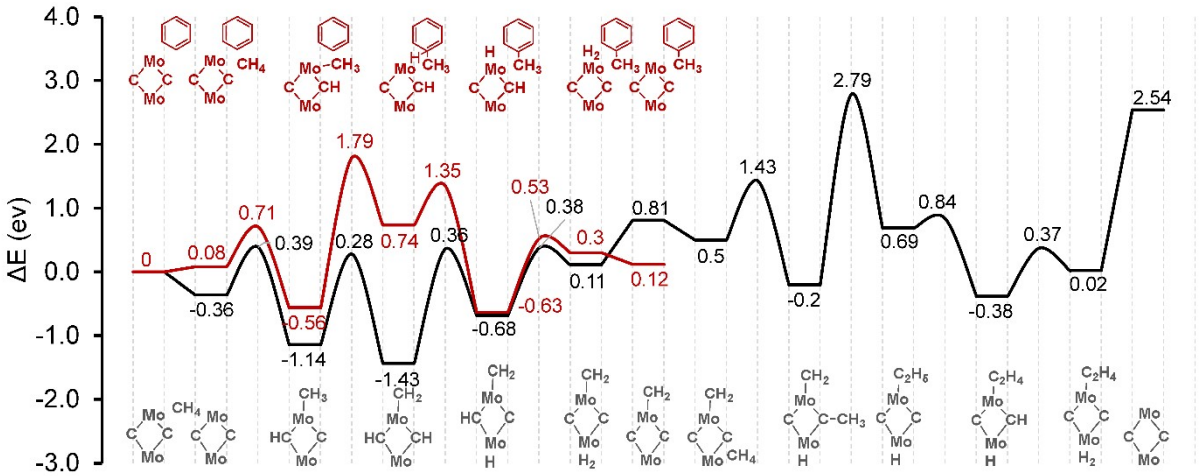

Figure S1. Reaction energy diagram of methane activation over $[Mo_2C_2]^{2+}$ located at β-site.

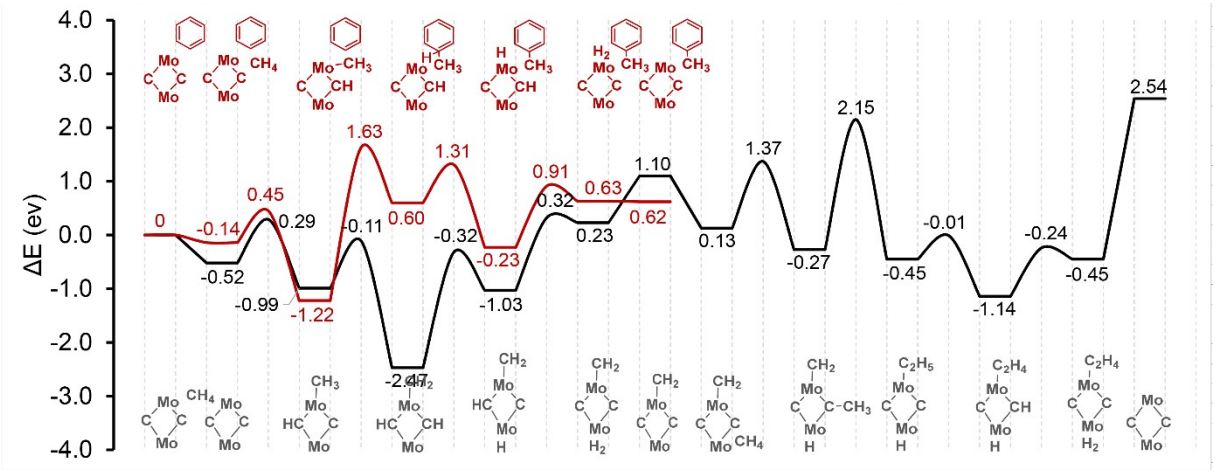

Figure S2. Reaction energy diagram of methane activation over $[Mo_2C_2]^{2+}$ located at γ-site.

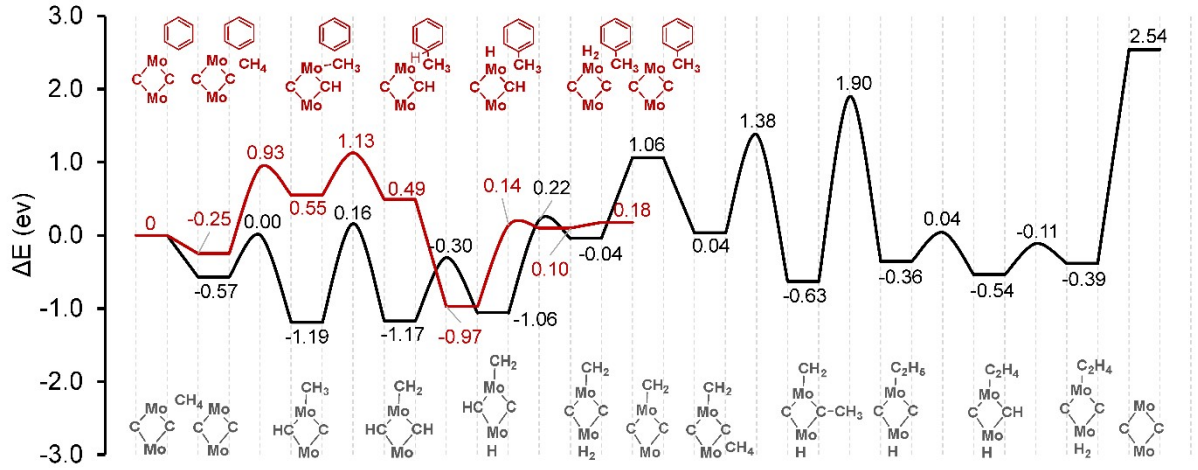

Figure S3. Reaction energy diagram of methane activation over $[Mo_2C_2]^{2+}$ located at δ-site.

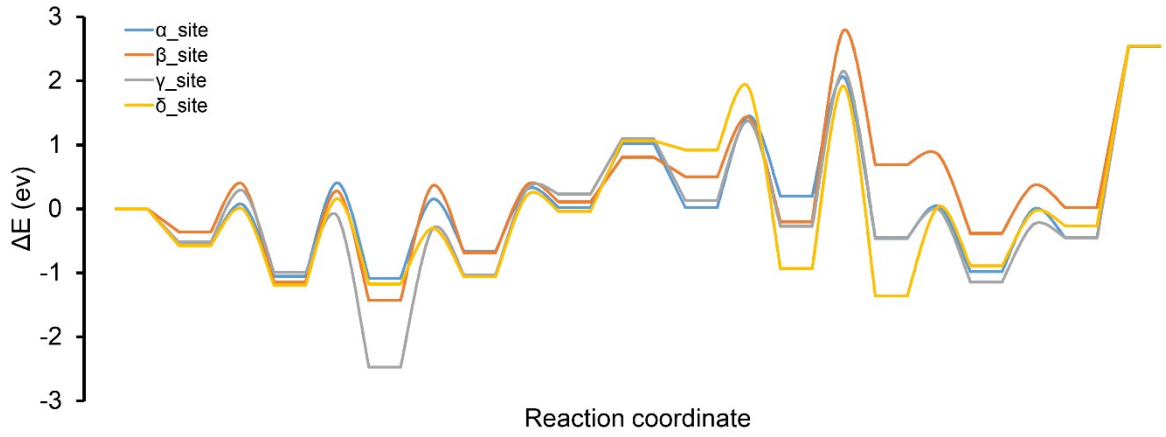

Figure S4. Comparison of methane activation over $[Mo_2C_2]^{2+}$ site located at various positions of ZSM-5 along ethylene formation pathway.

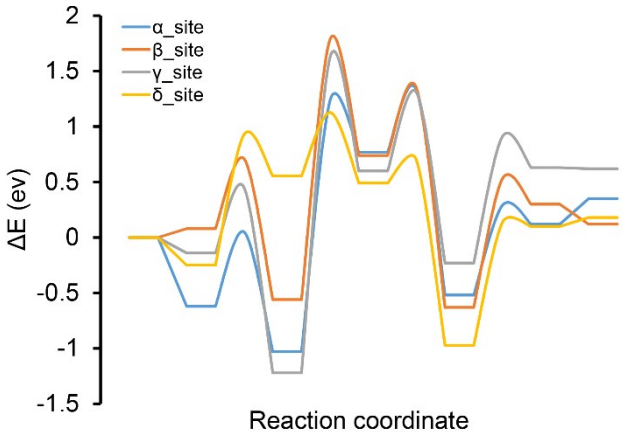

Figure S5. Comparison of methane activation over $[Mo_2C_2]^{2+}$ site located at various positions of ZSM-5 along hydrocarbon pool reaction pathway.

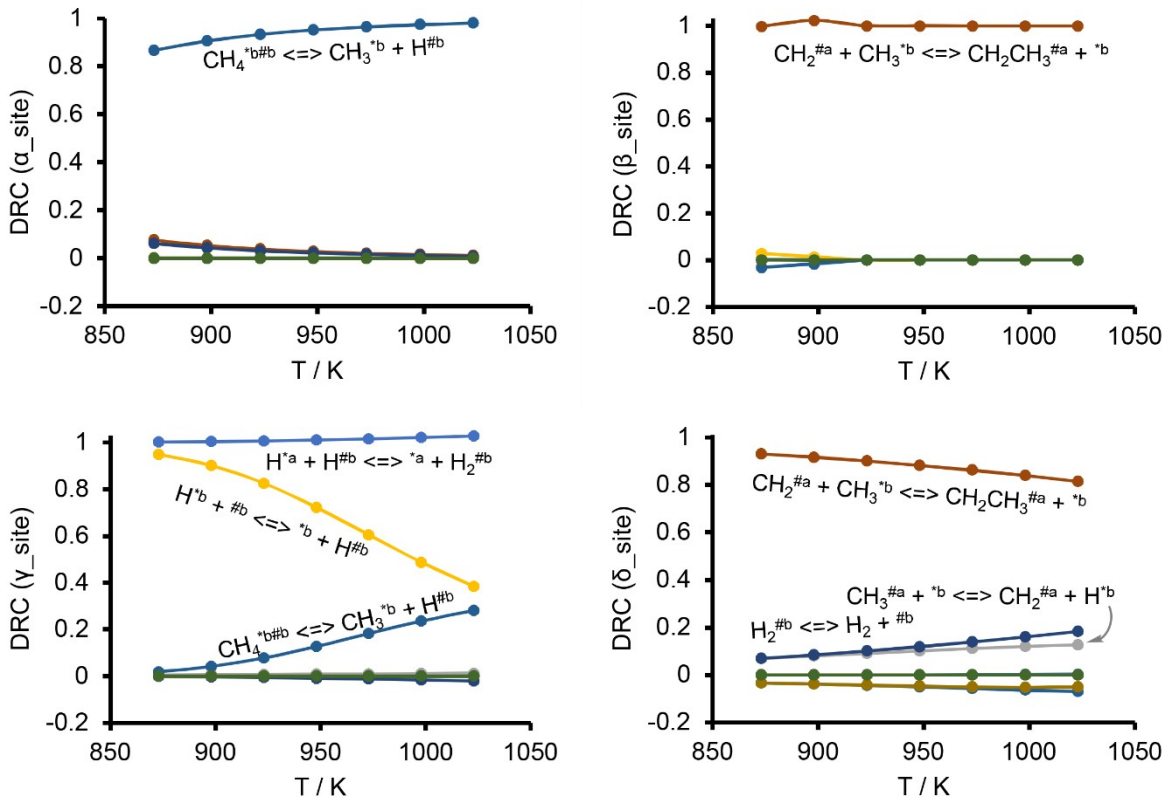

Figure S6. Calculated steady degree of rate control (DRC) analysis for methane activation over the $[Mo_2C_2]^{2+}$ site along ethylene pathways. Herein, * and # stand for the C and Mo sites of $[Mo_2C_2]^{2+}$, respectively.

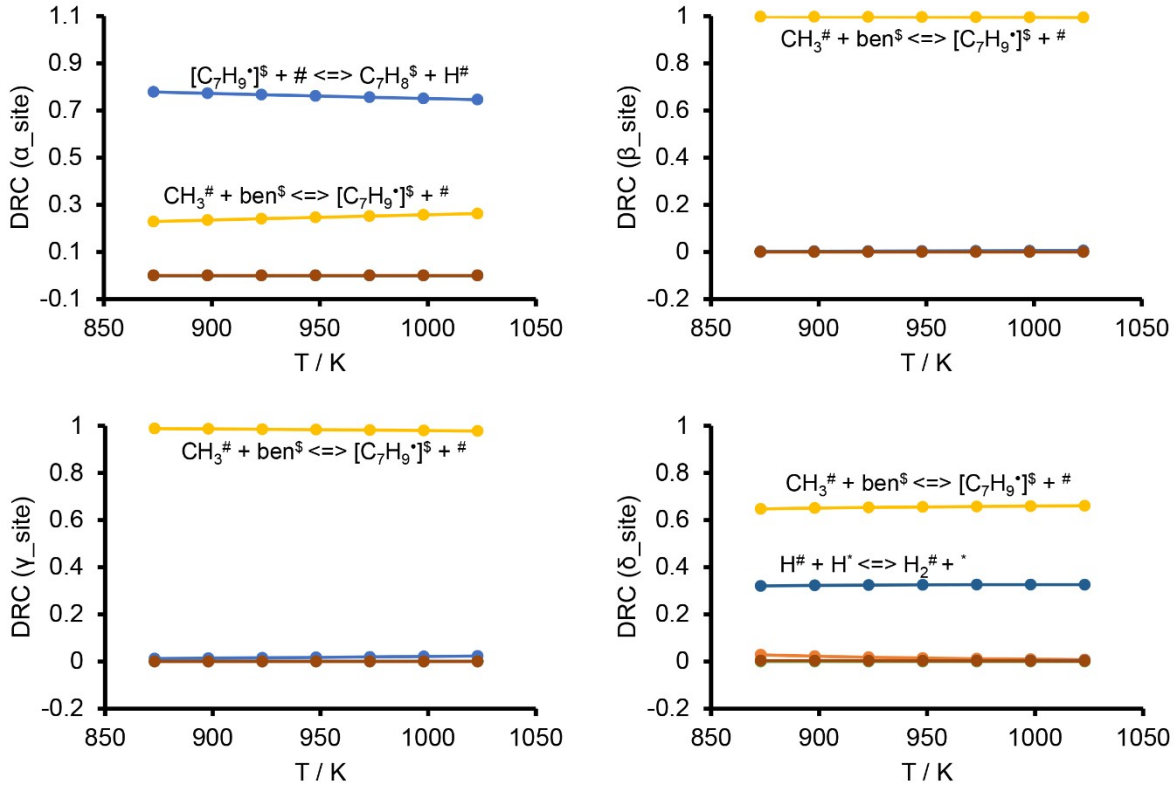

Figure S7. Calculated steady degree of rate control (DRC) analysis for methane activation over the $[Mo_2C_2]^{2+}$ site along hydrocarbon pool pathways. Herein, * and # stand for the C and Mo sites of $[Mo_2C_2]^{2+}$, respectively.

α-site Reactant Transition State Product

Ethylene formation reaction pathway

Step 2

Step 3

Step 4

Step 5

Step 8

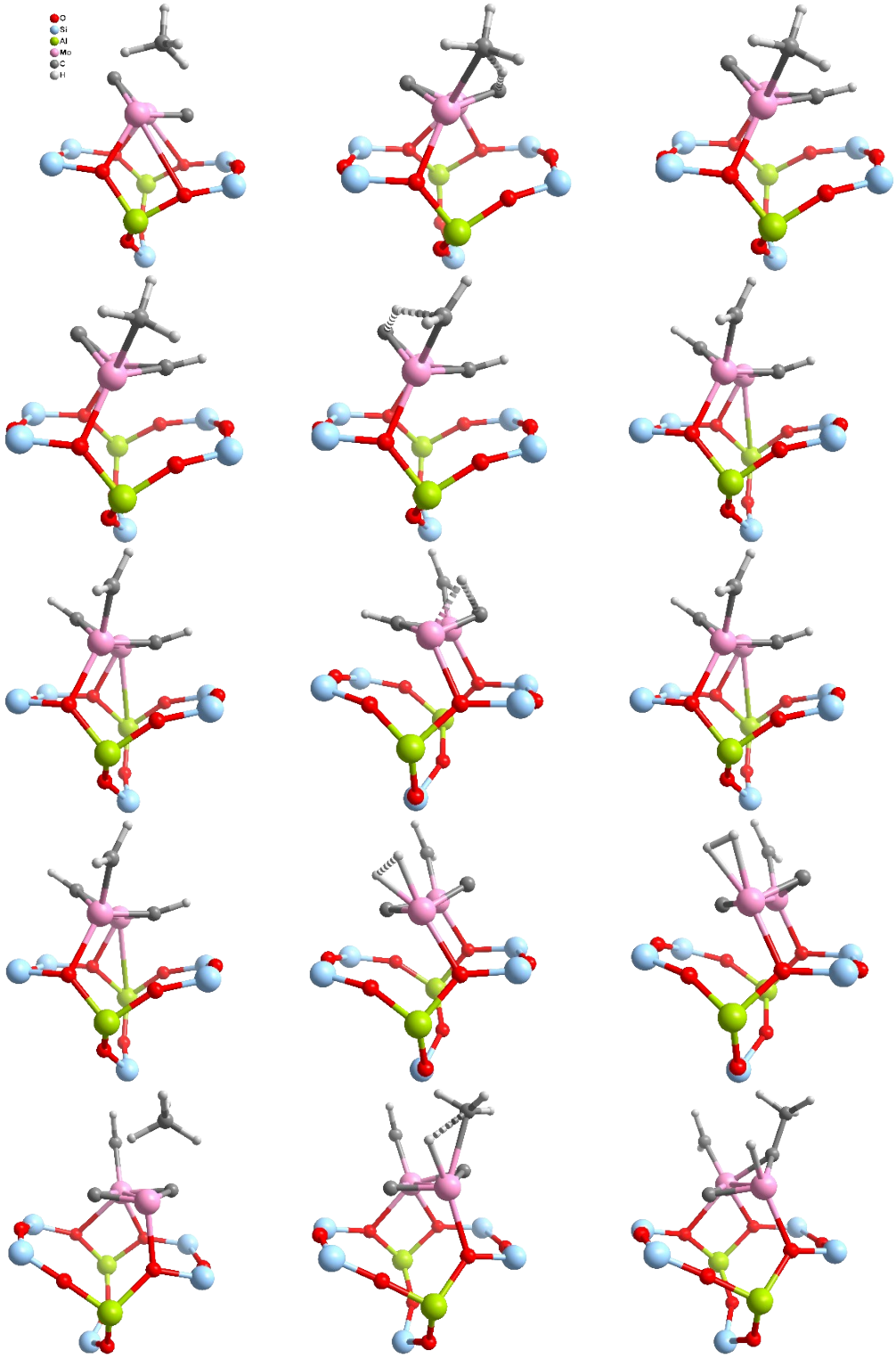

Step 9

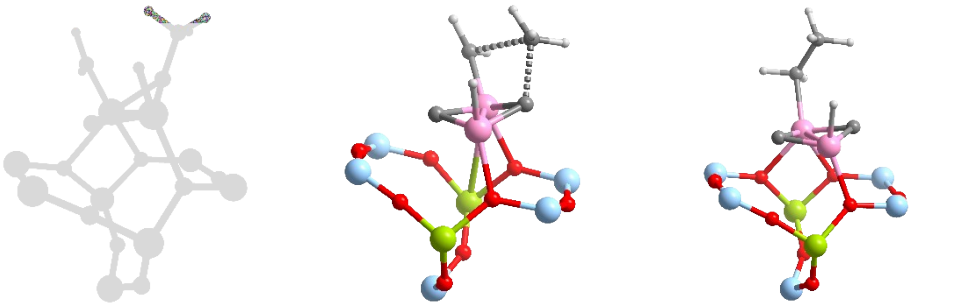

Step 10

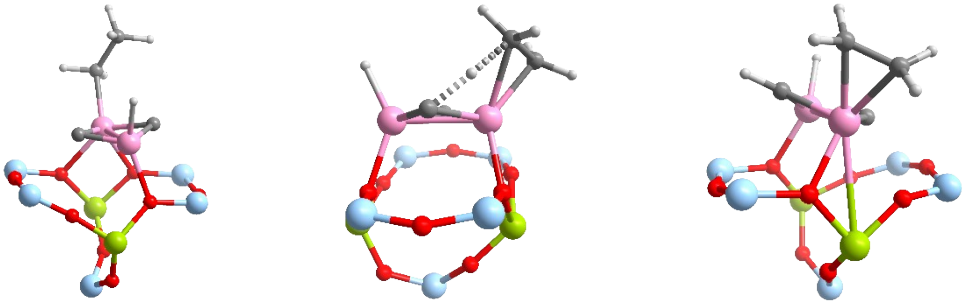

Step 11

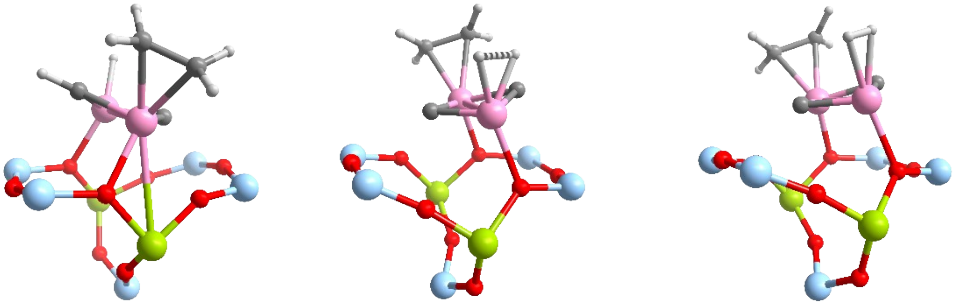

Hydrocarbon pool reaction pathway

Step 2

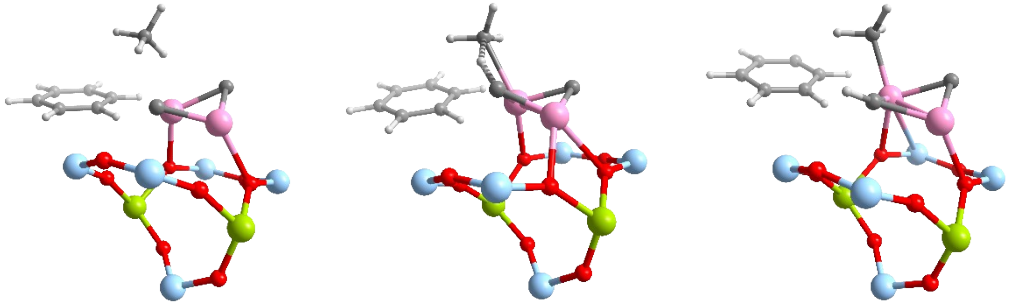

Step 3

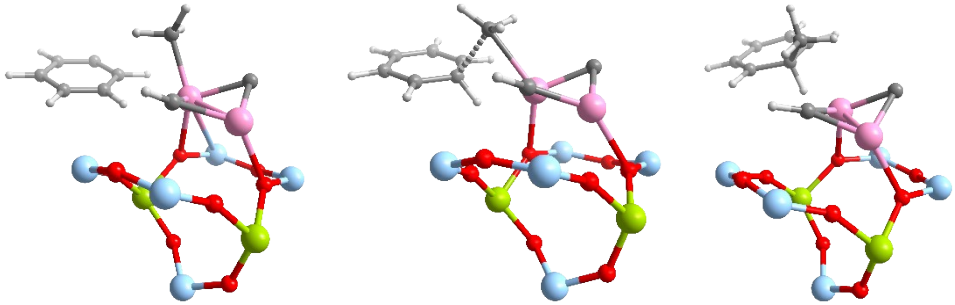

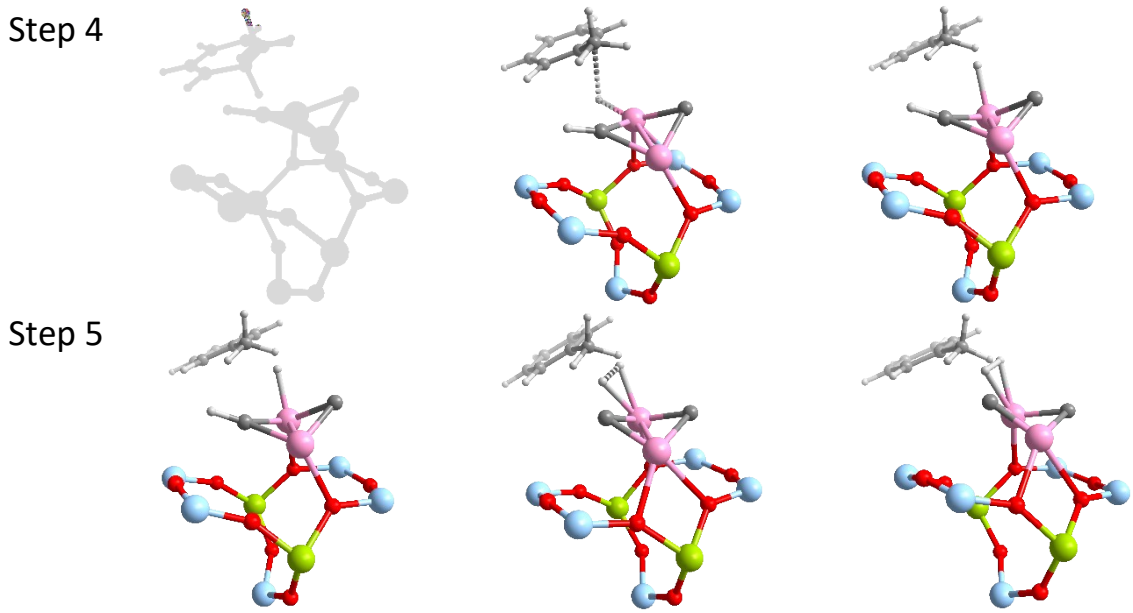

Figure S8. Local geometries of all transition states and selected key reaction intermediates for MDA reaction via both ethylene and hydrocarbon pool pathways over α-site (all reaction intermediates coordinates over four sites are provided in the separate coordinate_cif.zip file).

Table S1. Summarized reaction energy and activation barrier for all elementary reaction steps.

Elementary reaction steps		Reaction energy (ΔE, eV)[3]				Activation barrier(Ea, eV)[4]			
		α	β	γ	δ	α	β	γ	δ
Ethylene formation reaction pathway									
Step 1	CH_4[1]+*↔CH_4*	-0.57	-0.36	-0.52	-0.57	-	-	-	-
Step 2	CH_4*↔CH_3*+H*	-0.48	-0.78	-0.47	-0.62	0.64	0.75	0.81	0.57
Step 3	CH_3*↔CH_2*+H*	-0.03	-0.29	-1.48	0.02	1.46	1.42	0.88	1.35
Step 4	H*↔H_{shift}*	0.42	0.75	1.44	0.11	1.23	1.79	2.15	0.87
Step 5	2H*↔H_2*	0.68	0.79	1.26	1.02	0.97	1.06	1.35	1.28
Step 6	H_2*↔H_2	1.00	0.70	0.87	1.10	-	-	-	-
Step 7	CH_4[2]+*↔CH_4*	1.00	0.76	0.97	1.02	-	-	-	-
Step 8	CH_4*↔CH_3*+H*	0.18	-0.70	-0.40	-0.67	1.43	1.38	1.24	1.42
Step 9	CH_3*+CH_2*↔C_2H_5*	-0.48	0.71	-0.18	0.27	1.86	2.99	2.42	2.53
Step 10	C_2H_5*↔C_2H_4*+H*	-0.52	-1.07	-0.69	-0.18	0.50	0.15	0.44	0.40
Step 11	2H*↔H_2*	0.53	0.40	0.69	0.15	0.98	0.75	0.90	0.65
Step 12	C_2H_4*+H_2*↔C_2H_4+H_2	2.09	2.56	2.09	2.93	-	-	-	-
Hydrocarbon pool reaction pathway									
Step 1	CH_4+*↔CH_4*	-0.62	0.08	-0.14	-0.25	-	-	-	-
Step 2	CH_4*↔CH_3*+H*	-0.41	-0.64	1.08	0.80	0.67	0.63	0.59	1.18
Step 3	CH_3*+C_6H_6↔C_7H_9•	1.80	1.30	1.82	0.06	2.27	2.35	2.85	0.58
Step 4	C_7H_9•+*↔C_7H_8+H*	-1.29	-1.37	-0.83	-1.46	0.56	0.61	0.71	-
Step 5	2H*↔H_2*	0.64	0.60	0.86	1.07	0.81	1.16	1.14	1.11
Step 6	H_2*↔H_2	0.23	-0.18	-0.01	0.08	-	-	-	-

[1] First CH_4 activation

[2] Second CH_4 activation

[3] $\Delta E=E_{product}-E_{reactant}$, negative values indicate exothermic reactions

[4] $Ea=E_{TS}-E_{reactant}$

It is found that initial activation of the C-H bond of methane over the Mo_2C_2 site is more active than that over the Mo_4C_4 site proposed by Gao et al.[10] The activation barrier over Mo_4C_4 confined in the micropore of ZSM-5 was reported to be 112 kJ/mol, and reaction energy was -46 kJ/mol. While E_a and ΔE were 140 kJ/mol and -62 kJ/mol when Mo_4C_4 cluster was located at the external surface of ZSM-5. Table S1 indicates that for both reaction pathways, i.e., ethylene formation and hydrocarbon pool routes, the activation barriers are in the range of 60-80 kJ/mol, except the case of δ-site along hydrocarbon pool route (E_a = 118 kJ/mol). Zhou et al performed DFT studies of methane dehydrogenation and coupling to ethylene by using the model active sites of $Mo_2(CH_2)_5^{2+}$, $Mo_2(CH_2)_4^{2+}$, and $Mo(CH_2)_2CH_3^+$.[11] The activation energies of methane C−H bond dissociation over all $Mo(CH_2)_x$/HZSM-5 sites were between 101-202 kJ/mol, indicating the less active catalytic ability of these sits compared to Mo_2C_2. The activation barrier for H_2 formation over Mo_2C_2 site is found within 65-135 kJ/mol in this study,

while this step is less favorable over all $Mo(CH_2)_x$/HZSM-5 sites as well, featured with activation barriers ranging from 147 kJ/mol to 281 kJ/mol. Therefore, it is concluded that Mo_2C_2 species proposed in this study is both thermodynamically and kinetically preferable for MDA reaction.

References:

1. G. Kresse and J. Furthmüller, *Phys. Rev. B*, 1996, **54**, 11169-11186.
2. G. Kresse and D. Joubert, *Phys. Rev. B*, 1999, **59**, 1758-1775.
3. J. P. Perdew, K. Burke and M. Ernzerhof, *Phys. Rev. Lett.*, 1996, **77**, 3865-3868.
4. P. E. Blöchl, *Phys. Rev. B*, 1994, **50**, 17953-17979.
5. S. Grimme, S. Ehrlich and L. Goerigk, *J. Comput. Chem.*, 2011, **32**, 1456-1465.
6. G. Henkelman, B. P. Uberuaga and H. Jónsson, *J. Chem. Phys.*, 2000, **113**, 9901-9904.
7. H. van Koningsveld, J. C. Jansen and H. van Bekkum, *Zeolites*, 1990, **10**, 235-242.
8. A. H. Motagamwala and J. A. Dumesic, *Chem. Rev.*, 2021, **121**, 1049-1076.
9. C. T. Campbell, *J. Catal.*, 2001, **204**, 520-524.
10. J. Gao, Y. T. Zheng, J. M. Jehng, Y. D. Tang, I. E. Wachs and S. G. Podkolzin, *Science*, 2015, **348**, 686-690.
11. D. Zhou, S. Zuo and S. Xing, *J. Phys. Chem. C*, 2012, **116**, 4060-4070.